Metal surfaces catalyze polarization-dependent hydride transfer from H_2

Hai-Xu Wang
Massachusetts Institute of Technology https://orcid.org/0000-0003-0127-9544
Wei Lun Toh
Massachusetts Institute of Technology https://orcid.org/0000-0001-9001-0488
Bryan Tang
Massachusetts Institute of Technology
Yogesh Surendranath (yogi@mit.edu)
Massachusetts Institute of Technology https://orcid.org/0000-0003-1016-3420

Article

Keywords:

Posted Date: October 26th, 2022

DOI: https://doi.org/10.21203/rs.3.rs-2162594/v1

Version of Record: A version of this preprint was published at Nature Catalysis on April 17th, 2023. See the published version at https://doi.org/10.1038/s41929-023-00944-1.

Abstract

Hydride transfer is a critical elementary reaction step that spans biological catalysis, organic synthesis, and energy conversion. Conventionally, hydride transfer reactions are carried out using (bio)molecular hydride reagents under homogeneous conditions. Herein, we report a conceptually distinct heterogeneous hydride transfer reaction via the net electrocatalytic hydrogen reduction reaction (HRR) which reduces H_2 to hydrides. The reaction proceeds by H_2 dissociative adsorption on a metal electrode to form surface M–H species, which are then negatively polarized to drive hydride transfer to molecular hydride acceptors with up to 95% Faradaic efficiency. We find that the hydride transfer reactivity of surface M–H species is highly tunable and its thermochemistry depends on the applied potential in a Nernstian fashion. Thus, depending on the electrode potential, we observe that the thermodynamic hydricity of Pt–H on the same Pt electrode can continuously span a range of >40 kcal mol^{-1}. This work highlights the critical role of electrical polarization on heterogeneous hydride transfer reactivity and establishes a sustainable strategy for accessing reactive hydrides directly from H_2.

Introduction

Hydride (H^-) transfer is a ubiquitous elementary reaction step that plays essential roles in biological catalysis,[1-3] organic synthesis,[4-6] and energy conversion.[7-11] Hydride transfer from molecular reagents is commonly employed and well established (Fig. 1a). In biology, hydride transfer from NADH and NADPH powers key substrate reduction reactions, including carbon fixation in the Calvin cycle.[1-3] In synthetic chemistry, a suite of organic and main group molecular hydride transfer reagents (e.g. aluminum hydrides, borohydrides, silanes) have been developed to carry out reduction reactions of common functional groups such as esters and ketones.[4] In energy catalysis, hydride transfer from transition metal complexes has been identified as a key step in CO_2 reduction.[7-10] The thermodynamic and kinetic profiles of hydride transfer reactions from molecular reagents have been extensively cataloged.[12-17] The free energy for hydride transfer is quantified by the thermodynamic hydricity (ΔG_{H^-}, defined as the free energy change associated with heterolytic cleavage of a hydride donor (HA) to form H^- and the corresponding hydride acceptor (A^+), Fig. 1a).[12,13] The thermodynamic hydricity is intrinsic to each hydride transfer reagent and can be systematically tuned by varying the chemical structure. Given the importance of hydride transfer reactions, new strategies for controlling the thermodynamic and kinetic landscape of reactive hydride species could be enabling for a wide array of chemical transformations.

In contrast to the well-explored homogeneous hydride transfer reactivity, heterogeneous hydride transfer at metal surfaces remains underexplored. Surface-bound hydrogen species (M − H) at metals such as platinum and palladium are often viewed as neutral H-atoms rather than hydrides,[18,19] and their H-atom transfer reactivities are well established in the context of nonpolar hydrogenation reactions of olefins[20] and in the recombination of M − H species to form H_2 as part of the electrochemical hydrogen evolution reaction (HER, Fig. 1b).[21] Surface M − H species can also undergo deprotonation in the context of the

hydrogen oxidation reaction (HOR, Fig. 1b).[21] In contrast to established H-atom and proton transfer reactivities, the hydride transfer reactivity of surface M − H is less studied. Nonetheless, surface hydride transfers have been invoked as part of polar (de)hydrogenation/hydrogenolysis and CO_2 reduction reactions.[22–33] Additionally, the electrochemical Heyrovsky step ($M - H + H^+ + e^- \rightarrow H_2$) in the HER can be equivalently viewed either as a proton-coupled electron transfer (PCET) to surface M − H,[21] or alternatively as an interfacial hydride transfer to a proton in solution. Given the rich ability of metal surfaces to generate surface M − H species via PCET or H_2 dissociative adsorption, a deeper exploration of the hydride transfer reactivity of surface M − H could offer new mechanistic insights and enable the development of novel surface-catalyzed transformations. However, the lack of understanding of factors controlling the thermodynamic hydricity of surface M − H (e.g. degree of polarization, choice of material) greatly impedes the systematic deployment of heterogeneous hydride transfer in catalysis.

To the best of our knowledge, there exists a paucity of experimental studies that directly examine heterogeneous hydride transfer reactivity. This knowledge gap stems, in large part, from the following challenges: 1) unlike molecular hydride reagents that are highly chemoselective, surface M − H can engage in competing side reactions including H-atom transfer and proton transfer (see above); 2) metal surfaces can also engage in other processes such as outer-sphere electron transfer (ET); 3) putative hydride transfer steps involving surface M − H are often embedded in overall catalytic sequences (e.g. HER, polar hydrogenation) and are, thus, difficult to isolate and quantify. Exposing the intrinsic thermodynamic and kinetic factors controlling interfacial hydride transfer requires the separation of this reaction step from other competing reactions. Owing to all these complexities, the hydride transfer reactivity of surface M − H has been primarily investigated by computational modeling,[26–30,33–36] rather than direct experiments.

Unambiguous studies of heterogeneous hydride transfer require 1) a mild and rapid method for the generation of surface M − H, and 2) reaction partners in solution that are selective for hydride transfer over other side reactions. Herein, we combine facile H_2 dissociation at metal electrodes with chemoselective molecular hydride acceptors (A^+) to isolate and demonstrate the hydride transfer reactivity of surface M − H species (Fig. 1c). These two steps together constitute a new electrochemical transformation, the hydrogen reduction reaction (HRR), where H_2 is, in net, reduced to two hydrides. We examine electrocatalytic heterogeneous hydride transfer to organic and organometallic substrates via HRR and quantify its thermodynamic and kinetic profiles. We find that, in stark contrast to a molecular hydride transfer reagent which has an intrinsic and fixed hydricity, a metal surface displays tunable thermodynamic hydricity that can be extrinsically controlled to span a wide range of > 40 kcal mol^{-1} in a continuous fashion (c.f. the difference between Super-Hydride® ($HBEt_3^-$) and NADH is ~ 35 kcal mol^{-1}),[13] depending on the degree of electrical polarization of the interface (Fig. 1c).

Results And Discussion

Reaction development

We first investigated the hydride transfer reactivity of Pt electrodes since Pt is known to rapidly form surface Pt – H species via H_2 dissociative adsorption. We chose the molecular hydride acceptor **BIM$^+$** (Fig. 2) as a model substrate for inducing interfacial hydride transfer reactivity since it has low reactivity toward hydrogenation or other potential side reactions with Pt – H,[37] and its outer-sphere one-electron reduction potential is relatively negative due to stabilization by aromaticity.[38] Under a N_2 atmosphere, the cyclic voltammogram of **BIM$^+$** in MeCN (black dashed trace in Fig. 2a) displays a one-electron reduction peak at – 2.01 V (unless otherwise stated, all potentials are referenced to the ferrocenium/ferrocene ($Fc^{+/0}$) redox couple). Upon purging the solution with H_2, we observed a new reductive peak at a more positive potential of – 1.58 V (red solid trace in Fig. 2a). The new peak had lower intensity when a Pt planar electrode or a Pt rotating disk electrode (RDE) was employed (Figs. S2 – S3), and is likely limited by H_2 transport due to its low solubility in MeCN (~ 3.5 mM).[39] This issue was addressed by using a Pt on polytetrafluoroethylene gas diffusion electrode (Pt/PTFE GDE, see SI for its preparation and cell design)[40] which was able to resist flooding of MeCN and greatly enhanced the intensity of the reductive peak (Fig. 2a). Constant potential electrolysis (CPE) of **BIM$^+$** under 1 atm of H_2 at – 1.75 V in a divided cell led to clean generation of the hydride transfer product **BIMH** (Fig. 2b) with 95% Faradaic efficiency (FE, Eq. 1 in Fig. 2) as quantified by NMR analysis. This observation indicates that the new voltammetric peak observed in the presence of H_2 corresponds to net hydride transfer to the substrate. A similar reactivity was also observed by using an organometallic hydride acceptor **IrCp$^+$** (Fig. 2).[41] The cyclic voltammogram of **IrCp$^+$** showed a new reductive peak when the atmosphere was switched from N_2 to H_2 (Fig. S6), and bulk electrolysis at the new peak also afforded the hydride transfer product **IrCpH** in 46% FE (Eq. 2 in Fig. 2). Control experiments revealed the essential role of both the Pt electrode and the applied polarization for inducing formation of **IrCpH** (see SI for details). The lower FE in this case is attributed to the lower stability of the **IrCpH** product[41] and also to the smaller separation in potential (~ 150 mV) between inner-sphere hydride transfer and outer-sphere ET to the complex (Fig. S6). These results suggest that, upon H_2 dissociation on the Pt electrode, electrical polarization can drive hydride transfer from surface Pt – H to molecular hydride acceptors, thereby constituting a net electrocatalytic hydrogen reduction reaction (HRR, general equation shown as Eq. 5 in Fig. 3). Notably, the hydride transfer potential for the weaker hydride acceptor, **BIM$^+$**, is more negative than that for the stronger hydride acceptor **IrCp$^+$**. Together, the data evince that Pt surfaces can catalyze the conversion of H_2 to reactive hydrides and that electrical polarization can be used to tune the hydride transfer reactivity.

Thermodynamic Studies

We performed thermodynamic studies of HRR to better understand the relationship between electrical polarization and interfacial hydride transfer reactivity. Given the reversibility of Pt-catalyzed interconversion of H_2 and H^+ in HER and HOR half-reactions, we postulated that Pt-catalyze HRR might also be reversible. If this is the case, the equilibrium potential of HRR will follow the Nernst equation (Eq. 6, in MeCN) which can be derived from Eqs. 3 – 5 in Fig. 3 (see SI for detailed derivation). Experimentally,

the equilibrium potential could be sampled as the open circuit potential (E_{OCP}). Eq. 6 expresses that E_{OCP} of HRR has a 59 mV/dec dependence on the concentration ratio of the conjugate hydride donor/acceptor pair, log ([A^+]/[HA]), and a 30 mV/dec dependence on the H_2 partial pressure, log p_{H2}. The standard potential for Eq. 5 is not a constant and depends on the choice of HA/A^+, and this is also reflected in Eq. 6 where E_{OCP} has a 43 mV/(kcal mol^{-1}) dependence on the thermodynamic hydricity of HA (Eq. 4, see SI for discussion). In the absence of any hydride acceptor, the standard potential for HRR (Eq. 3) can be calculated as $E^0_{H_2/H^-}$ = −3.37 V vs $Fc^{+/0}$ in MeCN from known literature values (see SI for derivation).[12] This potential is beyond the solvent window of MeCN, and addition of HA/A^+ can stabilize the hydride ion and positively shift the HRR potential to an experimentally accessible region.

Steady-state E_{OCP} values were first measured under 1 atm of H_2 and using MeCN as the solvent. We initially used **BIMH**/**BIM$^+$** as the hydride donor/acceptor pair owing to its high FE for hydride transfer (Eq. 1 in Fig. 2). The dependence of E_{OCP} on the concentration ratio was examined via two separate experiments (Fig. 3a): in one experiment the E_{OCP} values were measured at **BIMH**/**BIM$^+$** ratios from 10:1, 3:1, to 1:1 (25 mM each) by adding **BIM$^+$** into the solution, while in the other experiment they were measured at **BIMH**/**BIM$^+$** ratios from 1:10, 1:3, to 1:1 (25 mM each) by adding **BIMH**. The two E_{OCP} values at a 1:1 ratio of **BIMH**/**BIM$^+$** obtained from these two separate experiments agreed with each other (− 1.153 V and − 1.151 V), which implies the reversibility of the HRR system upon changing concentration ratios of HA/A^+. These values are also close to the theoretical value of − 1.19 V calculated for a 1:1 ratio of **BIMH**/**BIM$^+$** from the Nernst equation (Eq. 6). Moreover, the six data points return a slope of 57 ± 4 mV/dec as shown in Fig. 3a which is consistent with the 59 mV/dec scaling predicted by Eq. 6. The dependence of E_{OCP} on H_2 partial pressure was next examined by using a 1:1 mixture of **BIMH**/**BIM$^+$** (25 mM each). Reducing the H_2 partial pressure from 1 atm to 0.06 atm by dilution with Ar led to a monotonic decrease in E_{OCP} values by ~ 40 mV, and the slope of 31 ± 2 mV/dec also agrees well with the 30 mV/dec slope predicted by the Nernst equation (Fig. 3b). When the solution was again exposed to 1 atm H_2, the initially measured E_{OCP} value could be restored to within 5 mV, demonstrating the reversibility of the HRR system upon changing H_2 partial pressures. Finally, the dependence of E_{OCP} on ΔG_{H^-} was investigated by using a series of chemoselective molecular HA/A^+ pairs with known thermodynamic hydricity values[13] in a 1:1 ratio (25 mM each, Fig. 3c). For example, while **BIMH** with a hydricity of 50.1 kcal mol^{-1} afforded an E_{ocp} of − 1.15 V, a more positive E_{ocp} of − 0.70 V was obtained for the weaker hydride donor **HEH** with a hydricity of 61.5 kcal mol^{-1} (its E_{ocp} was also found to depend Nernstianly on the concentration ratio of **HEH**/**HE$^+$** as shown in Fig. S9). Across the four hydride donor/acceptor pairs examined, we observed a linear scaling with a slope of 40 ± 8 mV/(kcal mol^{-1}) which was again close to the theoretical value of 43 mV/(kcal mol^{-1}) in Eq. 6. These results indicate that E_{OCP} follows the Nernst equation for HRR (Eq. 6) and that HRR is a reversible process and the dominating electrochemical reaction under these conditions.

We note that this reversible HRR reactivity of Pt could offer a direct method for quantifying the thermodynamic hydricity, ΔG_{H^-}, of new molecular hydride reagents. Indeed, by setting up the HRR equilibrium and using Eq. 6, the E_{ocp} of a Pt electrode in contact with H_2 and the target HA/A^+ pair should provide a measurement of ΔG_{H^-}. This method could potentially allow for the simple and rapid determination of a wide range of hydricity values, and is complementary to current indirect methods that require a specific hydride donor that has close hydricity to the target HA (for the "hydride transfer method") or calculate hydricity by combining two or more constituent thermodynamic parameters (e.g. pK_a and two-electron redox potential, for the "potential-pK_a method").[12,13]

The observed dependence of E_{OCP} on ΔG_{H^-} (Fig. 3c) implies that surface Pt − H can equilibrate with HA/A^+ pairs with hydricity values spanning ~ 20 kcal mol^{-1} in MeCN. However, direct hydride transfer from HA to the nitrile group of MeCN impeded examination of particularly strong hydride donors in this solvent. Employing THF as a more inert solvent with respect to hydride addition, we found that surface Pt − H could equilibrate with hydride donors as strong as Super-Hydride®, $HBEt_3^-$ (Fig. 3d). Even for this particularly strong hydride donor, we observed the same Nernstian dependence of E_{OCP} on the donor/acceptor concentration ratio (Fig. S10). The data recorded in THF also display a roughly linear trend (Fig. 3d), but we refrain from interpreting the slope because the corresponding ΔG_{H^-} values in this plot are for MeCN solvent and are therefore only crude estimates of their authentic values in THF. Nonetheless, Figs. 3c – d collectively reveal that the hydricity of surface Pt − H can span > 40 kcal mol^{-1} and cover a wide spectrum of molecular hydride reagents, ranging from one of the strongest hydride donors (Super-Hydride®) to the mildly reactive NADH analogues (**HEH** and $\mathbf{AcrH_2}$).

Importantly, based on this thermodynamic relationship between electrode potential and ΔG_{H^-} (Figs. 3c – d), the hydricity of surface Pt − H ($\Delta G_{H^-,PtH}$) is expected to be directly dependent on potential, i.e. the electrical polarization of the interface. This is illustrated in Fig. 4: a more negative applied potential (left panel) raises the potential of Fermi level, E_F, of the electrode bearing surface M − H species, and thereby increases the driving force for hydride transfer to a given A^+ due to an increased electrostatic potential drop, $\Delta\phi$, at the interface. The quantitative relationship between surface M − H hydricity and electrode potential can be further understood by the thermochemical cycle shown in Fig. 5. For Pt or Pd electrodes, H_2 dissociative adsorption is nearly thermo-neutral, and thus the ΔG of HRR (ΔG_{HRR}, experimentally measured in Fig. 3) directly estimates ΔG_{H^-} for surface M − H ($\Delta G_{H^-,MH}$). According to the thermochemical cycle, $\Delta G_{H^-,MH}$ depends on the bond dissociation free energy of surface M − H ($BDFE_{MH}$), standard redox potential between solvated H-atom and solvated hydride $E(H\cdot/H^-)$, and E_F of the electrode (electrode potential). Because $E(H\cdot/H^-)$ is a constant[12] and $BDFE_{MH}$ is largely unaffected by potential,[42–45] E_F is the dominant variable in determining the $\Delta G_{H^-,MH}$ (Eq. 7 in Fig. 5). Such a potential-dependent hydricity is unique to heterogeneous hydride transfer and is in sharp contrast to molecular hydride transfer reagents which display fixed hydricity values encoded by their local electronic and structural features. Modifying the substituents on a molecular hydride donor can only give rise to discrete changes

in ΔG_{H^-} values, and the majority of previous experimental reports have shown that the range of molecular hydricity is generally much smaller than 40 kcal mol^{-1} for the derivatives of a given class of compounds.[12,13,46] In our system, Pt – H on the same Pt electrode can give rise to a range of $\Delta G_{H^-,PtH}$ exceeding 40 kcal mol^{-1} (Fig. 3c – d), and our thermodynamic analysis highlights that, by changing the degree of external electrical polarization, a continuum of hydricity values with a much larger range should also be accessible without altering the catalyst. This implies that the HRR system is capable of achieving higher reactivity than molecular hydride reagents, and that the continuous control of hydricity is potentially useful for providing unique selectivities compared to previous homogeneous hydride transfer methods.

Furthermore, Eq. 7 can be generally applied to interfacial hydride transfer reactions beyond HRR. By measuring or computing the $BDFE_{MH}$ for a given surface and the $E(H\cdot/H^-)$ for a given solution medium, $\Delta G_{H^-,MH}$ (M here can be any atom on a metallic or semiconducting surface) in that medium can be calculated using Eq. 7 provided that E_F at the interface can be measured. Moreover, the linear scaling between hydricity and Fermi potential should hold, regardless of the atomic composition of the surface. Thus, this quantitative relationship provides a paradigm for predicting the thermochemistry and reactivity of hydride transfer steps embedded within more complex reaction sequences such as the (de)hydrogenation or hydrogenolysis of polar bonds and the activation of small molecules such as CO_2.[22–33, 47]

Kinetic Studies

We next investigated the kinetics of HRR in MeCN using **BIM^+** as the model substrate. Given the reversible nature of HRR, its exchange current density (j_0) was measured by electrochemical impedance spectroscopy (EIS) near the equilibrium potential (E_{OCP}) under 1 atm of H_2 and using a 1:1 mixture of **BIM^+**/**BIMH** (25 mM each, Eq. 8 in Fig. 6). In order to facilitate EIS measurements, a platinized Pt electrode with a high electrochemically active surface area (ECSA, roughness factor = 90) was used to increase the exchange current (i_0) and decrease the charge transfer resistance (R_{CT}, Eq. 9 in Fig. 6). The Nyquist plot (Fig. 6b, black) obtained by EIS measurement could be well modelled by a Randles circuit containing a Warburg impedance (Fig. 6a). This analysis returns a calculated j_0 = 5.34 ± 0.24 μA cm^{-2} by Eq. 9. Decreasing the concentrations of **BIM^+** and **BIMH** led to lower j_0 values (Figs. S13 – S14), indicating that **BIM^+** and **BIMH** participate in the measured charge transfer process. When deuterated substrates D_2 and **BIMD** were used, a larger R_{CT} was observed, corresponding to a kinetic isotope effect (KIE) of 3.8 ± 0.4 (Fig. 6b, blue). This observation implies that the transfer of H species gates the rate of the measured electrochemical reaction. Collectively, these results suggest that the electrochemical HRR is responsible for the R_{CT} component in our EIS measurements and agree with the above data indicating that HRR is the dominant electrochemical reaction under these conditions. The relatively small j_0 value for HRR is in line with the known sluggishness of homogeneous hydride transfer reactions,[13,14] and the KIE for HRR of

BIM^+/BIMH is also within the range of KIE values measured for molecular hydride reagents (1.7 – 9.5).[48,49] Additionally, the lack of a separate R_{CT} component in the impedance spectra associated with adsorption pseudocapacitance[50] suggests that the surface Pt – H species are formed by the non-electrochemical H_2 dissociation rather than any electrochemical PCET processes. Together, these kinetic studies suggest that the HRR mechanism proceeds via H_2 dissociative adsorption, followed by rate-limiting hydride transfer to the molecular acceptor.

In addition, we compared the reaction kinetics between interfacial hydride transfer in HRR and interfacial proton transfer in HER/HOR. Hydride and proton transfer constitute the two main potential-dependent half reactions involving surface Pt – H species. **$TEAH^+$/TEA** was used as the proton donor/acceptor pair for HER/HOR[51] (Fig. 6c) and it showed a similar equilibrium potential to that of HRR with **BIM^+/BIMH** ($E_{OCP} \approx -1.2$ V for both reactions). Due to the faster kinetics of HER/HOR,[50] a planar Pt electrode with lower ECSA (roughness factor = 2) was employed. Under 1 atm H_2 and a 1:1 mixture of **$TEAH^+$/TEA** (25 mM each), a j_0 value of 6.27 ± 0.07 μA cm^{-2} was extracted for HER/HOR (Fig. 6c, blue), and the relatively slow reaction rate in MeCN has also been reported in the literature.[51–53] Similar to HRR, the observation of a single semicircle suggests that surface Pt – H species for HOR are also formed by the non-electrochemical H_2 dissociation (see above). Using the same planar Pt electrode, HRR of **BIM^+/BIMH** (Fig. 6c, black) exhibited a lower j_0 of 1.02 ± 0.09 μA cm^{-2}, which is of the same order of magnitude as that measured on the platinized Pt electrode (Fig. 6b, black). Since both HRR and HOR are likely initiated by dissociative adsorption of H_2 on Pt, the lower j_0 for HRR indicates that proton transfer from Pt – H to **$TEAH^+$/TEA** is more facile than hydride transfer to **BIM^+/BIMH** and that HRR of **BIM^+/BIMH** is not limited by H_2 transport or its dissociative adsorption. We stress that the observed differences in j_0 values likely arise from many factors including 1) differences in the steric or electrostatic (**BIM^+** has a charge of + 1; **TEA** is uncharged) profile of the acceptor; 2) differences in the intrinsic self-exchange rate constant[13,54] for the proton-/hydride-accepting atoms (carbon for **BIM^+** and nitrogen for **TEA**; and 3) differences in the ability of each donor/acceptor to pre-associate with surface active sites. Given these many complexities, the observation that the measured j_0 values for HRR and HER/HOR are within an order of magnitude of each other suggests that the kinetics of these two reactions are not drastically different at metal interfaces.

We also investigated the effect of electrode material on HRR kinetics. Planar Pd, Ni, and Au electrodes were selected to compare to the kinetic data on the planar Pt electrodes (Fig. 6c, black). It was found that the HRR equilibrium could be established on all these electrodes as their E_{OCP} values closely matched the equilibrium potential of − 1.2 V. Applying the same EIS analysis, we extracted the exchange current density for HRR on each material (Fig. 7, see SI for raw EIS data, fits, and full experimental details). EIS data evince that Pt is the most active electrode material among this family. Intriguingly, the exchange current density for Pd, 0.048 ± 0.02 μA cm^{-2}, is similar to that of Au, 0.046 ± 0.06 μA cm^{-2}. Au is known to be more sluggish at H_2 dissociation and contains a lower coverage of surface-adsorbed H species than

Pd under 1 atm of H_2, and this arises because the BDFE of Au – H is 6 – 8 kcal mol^{-1} lower than that of Pd – H.[18,19] However, since Au and Pd are both pinned to the same equilibrium potential of the overall HRR reaction, the lower BDFE for Au – H makes it a 6 – 8 kcal mol^{-1} stronger hydride donor (lower ΔG_{H^-}) relative to Pd – H, according to Eq. 7. This enhanced hydride donor strength may compensate for a lower Au – H coverage and smaller H_2 splitting rate, leading to similar overall reaction rates for HRR on Pd and Au. This observation also suggests that bimetallic alloys containing metals separately optimized for H_2 dissociation and hydride transfer respectively, could be promising candidates for the design of improved HRR catalysts. The reaction rate may also depend on other effects such as the double layer effect caused by different metals due to changes in work function and potential of zero charge.[55] Another aspect of materials design concerns the dependence of HRR kinetics on catalyst size and surface structure. Our EIS data reveal that the more roughened platinized Pt electrode has higher catalytic activity than the planar Pt electrode (j_0 of 5.34 vs 1.02 μA cm^{-2}, Fig. 6b – c), suggesting that Pt – H species at edge/corner sites may be more active for hydride transfer than those on terraces. In aggregate, these kinetic studies highlight that many noble and base metal surfaces can engage in hydride transfer and that the kinetic profile of hydride transfer can be competitive with those of ubiquitous interfacial proton transfer reactions. Additionally, these studies provide the basis for a broader examination of how catalyst surface structure and solution composition can be used to tailor HRR and interfacial hydride transfer to target substrates.

Conclusion And Outlook

In summary, we have developed the electrocatalytic hydrogen reduction reaction (HRR) as a potentially general strategy of generating reactive hydrides directly from H_2 on metal surfaces. We found that HRR to organic and organometallic substrates can proceed with high selectivity and is catalyzed at the reversible limit on Pt electrodes. Taking advantage of reversible HRR catalysis, we isolated and uncovered the thermodynamic and kinetic profiles of interfacial hydride transfer reactivity. Unlike molecular hydride transfer reagents, which display fixed and discrete hydride transfer thermochemistry that is intrinsic to the chemical structure, we found that the free energy of hydride transfer from a metal surface is extrinsically tunable and determined by the degree of electrical polarization of the interface. Consequently, interfacial polarization leads to systematic and continuous variation in the thermodynamic hydricity on a common Pt electrode by > 40 kcal mol^{-1}. The kinetic profile of interfacial hydride transfer mirrors that of interfacial PCET with similar KIE values and comparable rate constants. Notably, we observed reversible hydride transfer reactivity across a range of metal surfaces, suggesting that this reactivity, and its polarization dependence, may be general across a wide array of materials. The reversibility of HRR on Pt provides a direct and simple analytical method for quantifying molecular hydricity using the Nernst equation (Eq. 6 in Fig. 3). The quantitative relationship between surface hydricity and Fermi potential (Eq. 7 in Fig. 5) can also be generalized to other heterogeneous hydride transfer steps, especially those that are challenging to be isolated from a complex reaction sequence.

By generating reactive hydrides directly from H_2, HRR has the potential to afford enhanced atom- and mass-efficiency compared to molecular hydride reagents. Indeed, the reactive hydrides found in molecular reagents are all ultimately sourced from H_2 as well. However, the synthetic route consists of first treating H_2 with a stoichiometric amount of a highly reducing alkali metal such as Na or Li, followed by subsequent transfer of these alkali metal hydrides to main group or transition metal acceptors. Alternative to this legacy reaction sequence, the findings in this work provide an efficient approach to accessing reactive hydrides directly from H_2 via HRR electrocatalysis and could substantially improve the atom- and step-economy and sustainability of hydride transfer reactions. Thus, this work enables a broader examination of HRR-derived hydride transfer reactivity in diverse contexts including organic synthesis,[6,23] CO_2 conversion,[9] hydrogen storage,[56,57] and biocatalysis (e.g. regeneration of biological hydride donors).[2,58,59]

Declarations

Data availability

The data that support the findings of this study are included in the published article (and its Supplementary Information) or available from the corresponding author on reasonable request.

Acknowledgement

We gratefully acknowledge Alex Radosevich for fruitful discussions. The authors thank the entire Surendranath Lab for their support and scientific discussions, with particular acknowledgment towards Deiaa Harraz, Max Hülsey, and Jaeyune Ryu for reviewing the manuscript. This work was supported primarily by the Air Force Office of Scientific Research (AFOSR) under award number FA9550-18-1-0420. H.-X.W. thanks the generous support from Croucher Fellowship.

Author Contributions

H.-X.W. and Y.S. conceived the research and developed experiments. H.-X.W. conducted the majority of the experiments. W.L.T. and B.Y.T. contributed to experimental design and data analysis. H.-X.W. and Y.S wrote the manuscript with input from all authors.

Competing Interests

The authors declare no competing financial interest.

References

1. Belenky, P., Bogan, K. L. & Brenner, C. NAD^+ metabolism in health and disease. Trends Biochem. Sci. **32**, 12–19 (2007).

2. Hollmann, F., Arends, I. W. C. E. & Holtmann, D. Enzymatic reductions for the chemist. Green Chem. **13**, 2285–2314 (2011).
3. Sellés Vidal, L., Kelly, C. L., Mordaka, P. M. & Heap, J. T. Review of NAD(P)H-dependent oxidoreductases: Properties, engineering and application. Biochim. Biophys. Acta - Proteins Proteom. **1866**, 327–347 (2018).
4. Deno, N. C., Peterson, H. J. & Saines, G. S. The Hydride-Transfer Reaction. Chem. Rev. **60**, 7–14 (1960).
5. An, X.-D. & Xiao, J. Recent advances in hydride transfer-involved C(sp^3)–H activation reactions. Org. Chem. Front. **8**, 1364–1383 (2021).
6. Wang, F. & Stahl, S. S. Electrochemical Oxidation of Organic Molecules at Lower Overpotential: Accessing Broader Functional Group Compatibility with Electron – Proton Transfer Mediators. Acc. Chem. Res. **53**, 561–574 (2020).
7. Waldie, K. M., Ostericher, A. L., Reineke, M. H., Sasayama, A. F. & Kubiak, C. P. Hydricity of Transition-Metal Hydrides: Thermodynamic Considerations for CO_2 Reduction. ACS Catal. **8**, 1313–1324 (2018).
8. Yang, J. Y., Kerr, T. A., Wang, X. S. & Barlow, J. M. Reducing CO_2 to HCO_2^- at Mild Potentials: Lessons from Formate Dehydrogenase. J. Am. Chem. Soc. **142**, 19438–19445 (2020).
9. Kumar, A., Semwal, S. & Choudhury, J. Emerging Implications of the Concept of Hydricity in Energy-Relevant Catalytic Processes. Chem. Eur. J. **27**, 5842–5857 (2021).
10. Dey, S., Masero, F., Brack, E., Fontecave, M. & Mougel, V. Electrocatalytic metal hydride generation using CPET mediators. Nature **607**, 499–506 (2022).
11. Ilic, S., Gesiorski, J. L., Weerasooriya, R. B. & Glusac, K. D. Biomimetic Metal-Free Hydride Donor Catalysts for CO_2 Reduction. Acc. Chem. Res. **55**, 844–856 (2022).
12. Wiedner, E. S. *et al.* Thermodynamic Hydricity of Transition Metal Hydrides. Chem. Rev. **116**, 8655–8692 (2016).
13. Ilic, S., Alherz, A., Musgrave, C. B. & Glusac, K. D. Thermodynamic and kinetic hydricities of metal-free hydrides. Chem. Soc. Rev. **47**, 2809–2836 (2018).
14. Mayr, H. & Patz, M. Scales of Nucleophilicity and Electrophilicity: A System for Ordering Polar Organic and Organometallic Reactions. Angew. Chem. Int. Ed. **33**, 938–957 (1994).
15. Hammes-Schiffer, S. Comparison of Hydride, Hydrogen Atom, and Proton-Coupled Electron Transfer Reactions. ChemPhysChem **3**, 33–42 (2002).
16. Yang, J.-D., Xue, J. & Cheng, J.-P. Understanding the role of thermodynamics in catalytic imine reductions. Chem. Soc. Rev. **48**, 2913–2926 (2019).
17. Brereton, K. R., Smith, N. E., Hazari, N. & Miller, A. J. M. Thermodynamic and kinetic hydricity of transition metal hydrides. Chem. Soc. Rev. **49**, 7929–7948 (2020).
18. Ferrin, P., Kandoi, S., Nilekar, A. U. & Mavrikakis, M. Hydrogen adsorption, absorption and diffusion on and in transition metal surfaces: A DFT study. Surf. Sci. **606**, 679–689 (2012).

19. Skúlason, E. *et al.* Modeling the Electrochemical Hydrogen Oxidation and Evolution Reactions on the Basis of Density Functional Theory Calculations. J. Phys. Chem. C **114**, 18182–18197 (2010).
20. Nishimura, S. *Handbook of heterogeneous catalytic hydrogenation for organic synthesis*. (Wiley, 2001).
21. Gileadi, E. *Physical electrochemistry: fundamentals, techniques and applications.* (Wiley, 2011).
22. Eisenstein, O. & Crabtree, R. H. Outer sphere hydrogenation catalysis. New J. Chem. **37**, 21–27 (2013).
23. Jin, W. *et al.* Catalytic Upgrading of Biomass Model Compounds: Novel Approaches and Lessons Learnt from Traditional Hydrodeoxygenation – a Review. ChemCatChem **11**, 924–960 (2019).
24. Liu, K., Qin, R. & Zheng, N. Insights into the Interfacial Effects in Heterogeneous Metal Nanocatalysts toward Selective Hydrogenation. J. Am. Chem. Soc. **143**, 4483–4499 (2021).
25. Aireddy, D. R. & Ding, K. Heterolytic Dissociation of H_2 in Heterogeneous Catalysis. ACS Catal. **12**, 4707–4723 (2022).
26. Nelson, R. C. *et al.* Experimental and Theoretical Insights into the Hydrogen-Efficient Direct Hydrodeoxygenation Mechanism of Phenol over Ru/TiO_2. ACS Catal. **5**, 6509–6523 (2015).
27. Wyvratt, B. M. *et al.* Reactivity of Hydrogen on and in Nanostructured Molybdenum Nitride: Crotonaldehyde Hydrogenation. ACS Catal. **6**, 5797–5806 (2016).
28. Cai, H., Schimmenti, R., Nie, H., Mavrikakis, M. & Chin, Y.-H. C. Mechanistic Role of the Proton–Hydride Pair in Heteroarene Catalytic Hydrogenation. ACS Catal. **9**, 9418–9437 (2019).
29. Shangguan, J. *et al.* The Role of Protons and Hydrides in the Catalytic Hydrogenolysis of Guaiacol at the Ruthenium Nanoparticle–Water Interface. ACS Catal. **10**, 12310–12332 (2020).
30. Bender, M. T., Lam, Y. C., Hammes-Schiffer, S. & Choi, K.-S. Unraveling Two Pathways for Electrochemical Alcohol and Aldehyde Oxidation on NiOOH. J. Am. Chem. Soc. **142**, 21538–21547 (2020).
31. Barton, E. E., Rampulla, D. M. & Bocarsly, A. B. Selective Solar-Driven Reduction of CO_2 to Methanol Using a Catalyzed p-GaP Based Photoelectrochemical Cell. J. Am. Chem. Soc. **130**, 6342–6344 (2008).
32. Zeitler, E. L. *et al.* Isotopic Probe Illuminates the Role of the Electrode Surface in Proton Coupled Hydride Transfer Electrochemical Reduction of Pyridinium on Pt(111). J. Electrochem. Soc. **162**, H938-H944 (2015).
33. Xu, S. & Carter, E. A. Theoretical Insights into Heterogeneous (Photo)electrochemical CO_2 Reduction. Chem. Rev. **119**, 6631–6669 (2019).
34. Li, L., Martirez, J. M. P. & Carter, E. A. Identifying an Alternative Hydride Transfer Pathway for CO_2 Reduction on CdTe(111) and $CuInS_2$(112) Surfaces. Adv. Theory Simul. **5**, 2100413 (2022).
35. Jung, O., Jackson, M. N., Bisbey, R. P., Kogan, N. E. & Surendranath, Y. Innocent buffers reveal the intrinsic pH- and coverage-dependent kinetics of the hydrogen evolution reaction on noble metals. Joule **6**, 476–493 (2022).

36. Warburton, R. E., Soudackov, A. V. & Hammes-Schiffer, S. Theoretical Modeling of Electrochemical Proton-Coupled Electron Transfer. Chem. Rev. **122**, 10599–10650 (2022).
37. Kunnen, K., Nikonov, G. & Yunnikova, L. 1,3-Dimethyl-2-phenylbenzimidazoline. Encycl. Reagents Org. Synth., 1–3 (2014).
38. Zhu, X.-Q., Zhang, M.-T., Yu, A., Wang, C.-H. & Cheng, J.-P. Hydride, Hydrogen Atom, Proton, and Electron Transfer Driving Forces of Various Five-Membered Heterocyclic Organic Hydrides and Their Reaction Intermediates in Acetonitrile. J. Am. Chem. Soc. **130**, 2501–2516 (2008).
39. Purwanto, Deshpande, R. M., Chaudhari, R. V. & Delmas, H. Solubility of Hydrogen, Carbon Monoxide, and 1-Octene in Various Solvents and Solvent Mixtures. J. Chem. Eng. Data **41**, 1414–1417 (1996).
40. Dinh, C.-T., García de Arquer, F. P., Sinton, D. & Sargent, E. H. High Rate, Selective, and Stable Electroreduction of CO_2 to CO in Basic and Neutral Media. ACS Energy Lett. **3**, 2835–2840 (2018).
41. Barrett, S. M., Pitman, C. L., Walden, A. G. & Miller, A. J. M. Photoswitchable Hydride Transfer from Iridium to 1-Methylnicotinamide Rationalized by Thermochemical Cycles. J. Am. Chem. Soc. **136**, 14718–14721 (2014).
42. Christmann, K. Interaction of hydrogen with solid surfaces. Surf. Sci. Rep. **9**, 1–163 (1988).
43. Sheng, W. *et al.* Correlating hydrogen oxidation and evolution activity on platinum at different pH with measured hydrogen binding energy. Nat. Commun. **6**, 5848 (2015).
44. Noh, H. & Mayer, J. M. Medium-independent hydrogen atom binding isotherms of nickel oxide electrodes. Chem (2022). DOI: 10.1016/j.chempr.2022.08.018.
45. Tang, B. Y., Bisbey, R. P., Lodaya, K. M., Toh, W. L. & Surendranath, Y. Reaction Environment Impacts Charge Transfer But Not Chemical Reaction Steps in Hydrogen Evolution Catalysis. *ChemRxiv*, DOI: 10.26434/chemrxiv-22022-26432ln26430 (2022).
46. Computational studies predicted a range of ~ 80 kcal mol^{-1} for tetra-substituted borohydrides: Heiden, Z. M. & Lathem, A. P. Establishing the Hydride Donor Abilities of Main Group Hydrides. *Organometallics* **34**, 1818–1827 (2015).
47. Ertem, M. Z., Konezny, S. J., Araujo, C. M. & Batista, V. S. Functional Role of Pyridinium during Aqueous Electrochemical Reduction of CO_2 on Pt(111). J. Phys. Chem. Lett. **4**, 745–748 (2013).
48. Kil, H. J. & Lee, I.-S. H. Primary Kinetic Isotope Effects on Hydride Transfer from Heterocyclic Compounds to NAD^+ Analogues. J. Phys. Chem. A **113**, 10704–10709 (2009).
49. Shen, G.-B. *et al.* Prediction of Kinetic Isotope Effects for Various Hydride Transfer Reactions Using a New Kinetic Model. J. Phys. Chem. A **120**, 1779–1799 (2016).
50. Ledezma-Yanez, I. *et al.* Interfacial water reorganization as a pH-dependent descriptor of the hydrogen evolution rate on platinum electrodes. Nat. Energy **2**, 17031 (2017).
51. Jackson, M. N. & Surendranath, Y. Donor-Dependent Kinetics of Interfacial Proton-Coupled Electron Transfer. J. Am. Chem. Soc. **138**, 3228–3234 (2016).
52. Ledezma-Yanez, I. & Koper, M. T. M. Influence of water on the hydrogen evolution reaction on a gold electrode in acetonitrile solution. J. Electroanal. Chem. **793**, 18–24 (2017).

53. Mikolajczyk, T., Luba, M., Pierozynski, B. & Smoczynski, L. A Detrimental Effect of Acetonitrile on the Kinetics of Underpotentially Deposited Hydrogen and Hydrogen Evolution Reaction, Examined on Pt Electrode in H_2SO_4 and NaOH Solutions. Catalysts **10**, 625 (2020).
54. Mayer, J. M. Understanding Hydrogen Atom Transfer: From Bond Strengths to Marcus Theory. Acc. Chem. Res. **44**, 36–46 (2011).
55. Ludwig, T., Singh, A. R. & Nørskov, J. K. Acetonitrile Transition Metal Interfaces from First Principles. J. Phys. Chem. Lett. **11**, 9802–9811 (2020).
56. Zidan, R. *et al.* Aluminium hydride: a reversible material for hydrogen storage. Chem. Commun., 3717–3719 (2009).
57. Demirci, U. B. & Miele, P. Sodium borohydride versus ammonia borane, in hydrogen storage and direct fuel cell applications. Energy Environ. Sci. **2**, 627–637 (2009).
58. Wu, H. *et al.* Methods for the regeneration of nicotinamide coenzymes. Green Chem. **15**, 1773–1789 (2013).
59. Wang, X. *et al.* Cofactor NAD(P)H Regeneration Inspired by Heterogeneous Pathways. Chem **2**, 621–654 (2017).

Figures

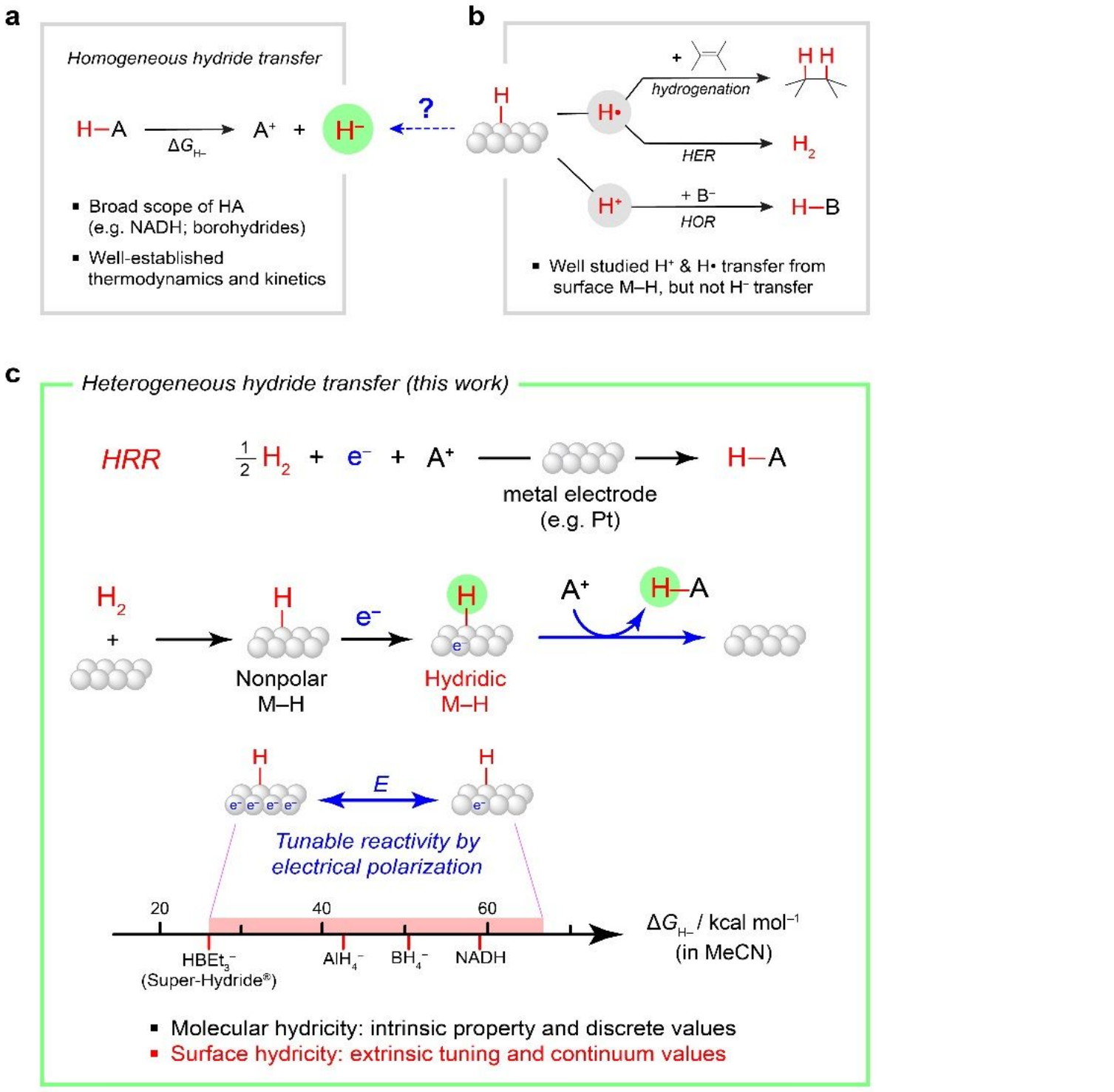

Figure 1

Reaction design. a, Homogeneous hydride transfer reactions using molecular hydride reagents have been extensively studied. HA = molecular hydride donor; ΔG_{H-} = thermodynamic hydricity. **b**, H-atom transfer and proton transfer reactivities of surface M–H species are well documented, yet their hydride transfer reactivity remains poorly understood. HER = hydrogen evolution reaction; HOR = hydrogen oxidation reaction; B^- = proton acceptor. **c**, This work: heterogeneous hydride transfer via electrocatalytic hydrogen

reduction reaction (HRR) which, in net, reduces H_2 to hydrides (top) and tunable hydricity of surface M–H by electrical polarization (bottom).

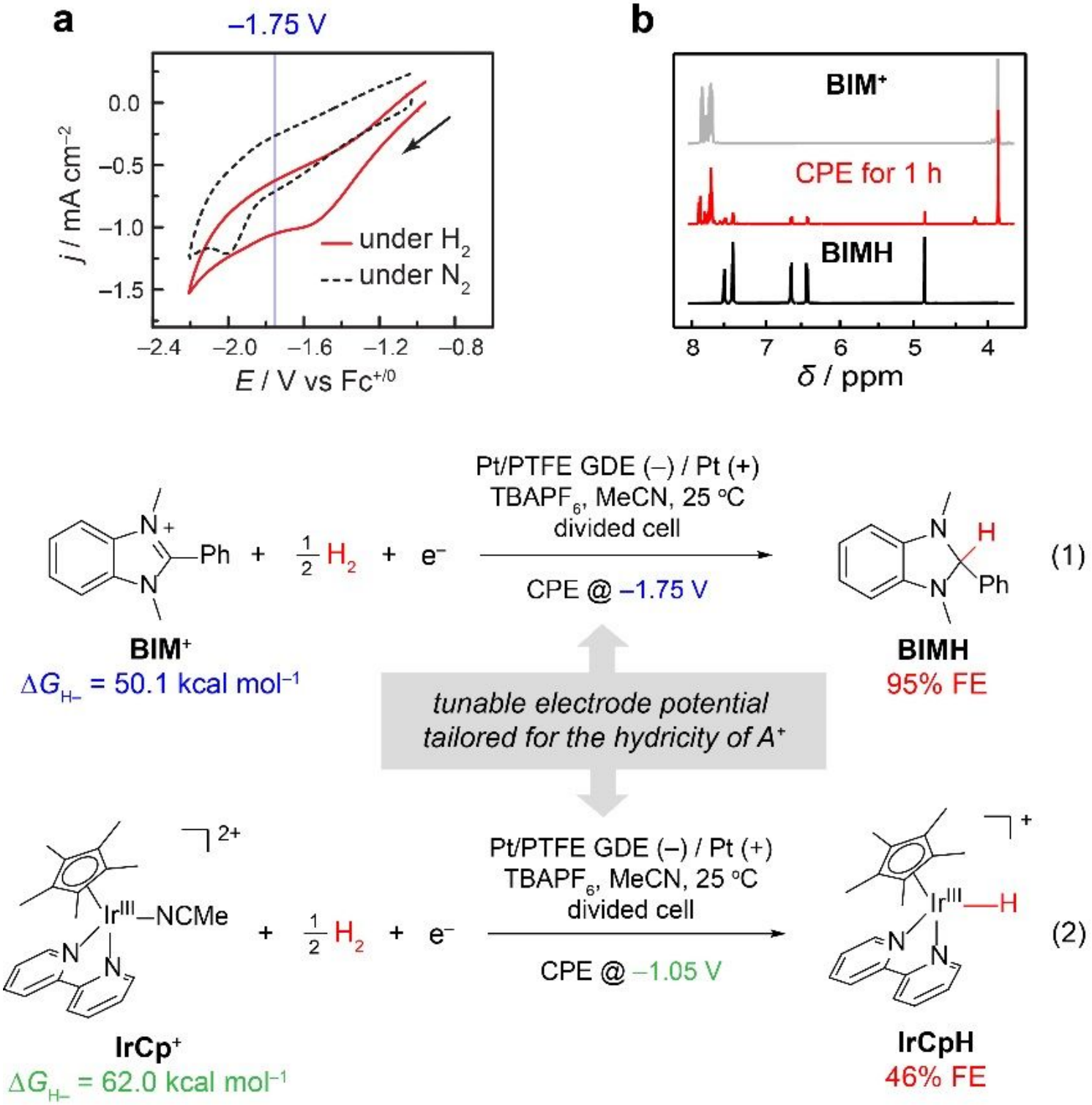

Figure 2

Heterogeneous hydride transfer via electrocatalytic hydrogen reduction reaction (HRR). a, Cyclic voltammograms of **BIM$^+$** under N_2 (black dashed trace) and H_2 (red solid trace). Conditions: 5 mM **BIM$^+$**,

0.2 M tetrabutylammonium hexafluorophosphate ($TBAPF_6$), 1 atm N_2 or H_2, MeCN, 100 mV/s scan rate, 25 °C, collected using Pt/PTFE GDE as the working electrode. **b**, Crude ^1H NMR spectrum (in CD_3CN) of constant potential electrolysis (CPE) of **BIM$^+$** at −1.75 V for 1 h (red trace) showed the formation of **BIMH**. Bottom: chemical equations for HRR of **BIM$^+$** (eq. 1) and **IrCp$^+$** (eq. 2). All potentials are referenced to ferrocenium/ferrocene ($Fc^{+/0}$) redox couple. See SI for detailed cell design, reaction conditions, and Faraday efficiency (FE) determination.

$$\tfrac{1}{2}H_2 + e^- \overset{E^0_{H_2/H^-}}{\rightleftharpoons} H^- \quad (3)$$

$$(-)\qquad H{-}A \overset{\Delta G_{H-}}{\rightleftharpoons} A^+ + H^- \quad (4)$$

$$\textit{HRR}\qquad A^+ + \tfrac{1}{2}H_2 + e^- \rightleftharpoons H{-}A \quad (5)$$

Nernst Equation for HRR

$$E_{ocp} = E^0_{H_2/H^-} + \frac{2.3RT}{F}\log\frac{[A^+]}{[HA]} + \frac{2.3RT}{2F}\log p_{H_2} + \frac{1}{F}\Delta G_{H-} \quad (6)$$

$$= -3.37 + 0.059\log\frac{[A^+]}{[HA]} + 0.030\log p_{H_2} + 0.043\,\Delta G_{H-}$$

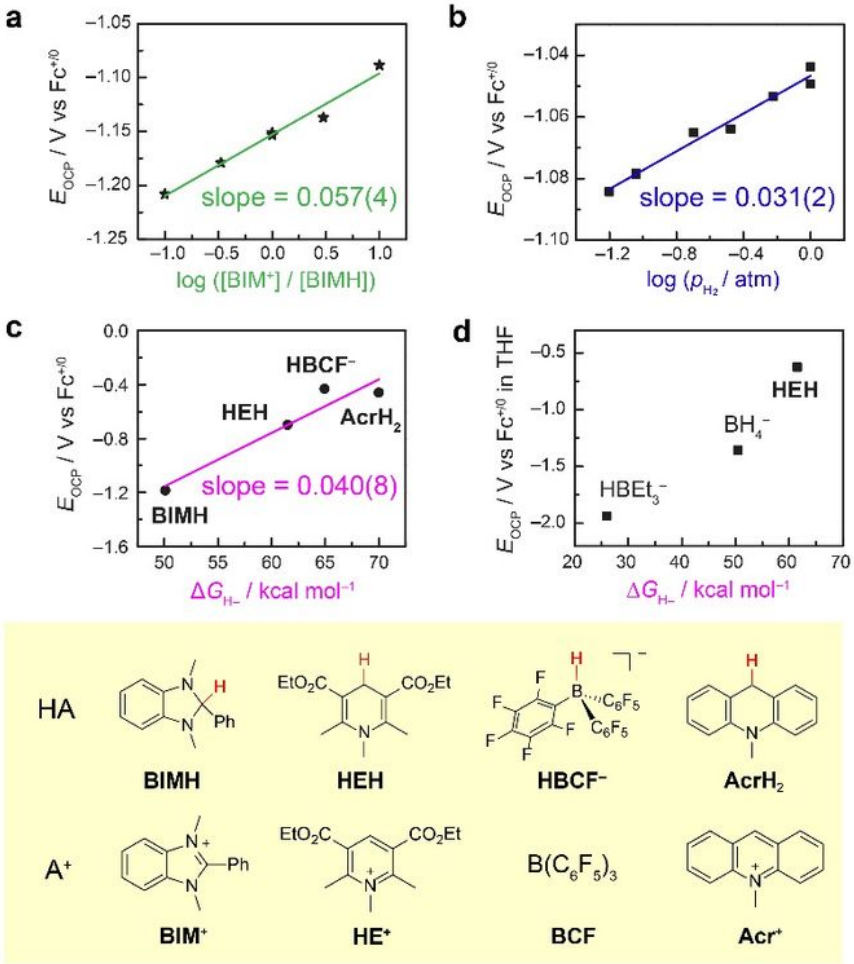

Figure 3

Thermodynamic studies. The Nernst equation for HRR in MeCN (eq. 6) was derived from a thermochemical cycle (eqs. 3–5) and probed experimentally (**a**–**c**), which demonstrate the reversibility of HRR on Pt electrodes. = standard reduction potential between H_2 gas and solvated hydride ion. F = Faraday's constant; R = gas constant; T = temperature. **a**, Dependence of E_{OCP} on the concentration ratio (from 1:10 to 10:1) between **BIM**$^+$ and **BIMH**. **b**, Dependence of E_{OCP} on H_2 partial pressure (p_{H2}, from 0.06 to 1 atm). **c**, Dependence of E_{OCP} on the thermodynamic hydricity of HA/A^+ pair (HA = **BIMH**, **HEH**, **HBCF**$^-$, and **AcrH$_2$**). **d**, Dependence of E_{OCP} in THF on the thermodynamic hydricity of HA/A^+ pair (HA = **HBEt$_3$**$^-$, **BH$_4$**$^-$, and **HEH**, ΔG_{H^-} values are in MeCN and thus no linear correlation is made here). See SI for experimental details.

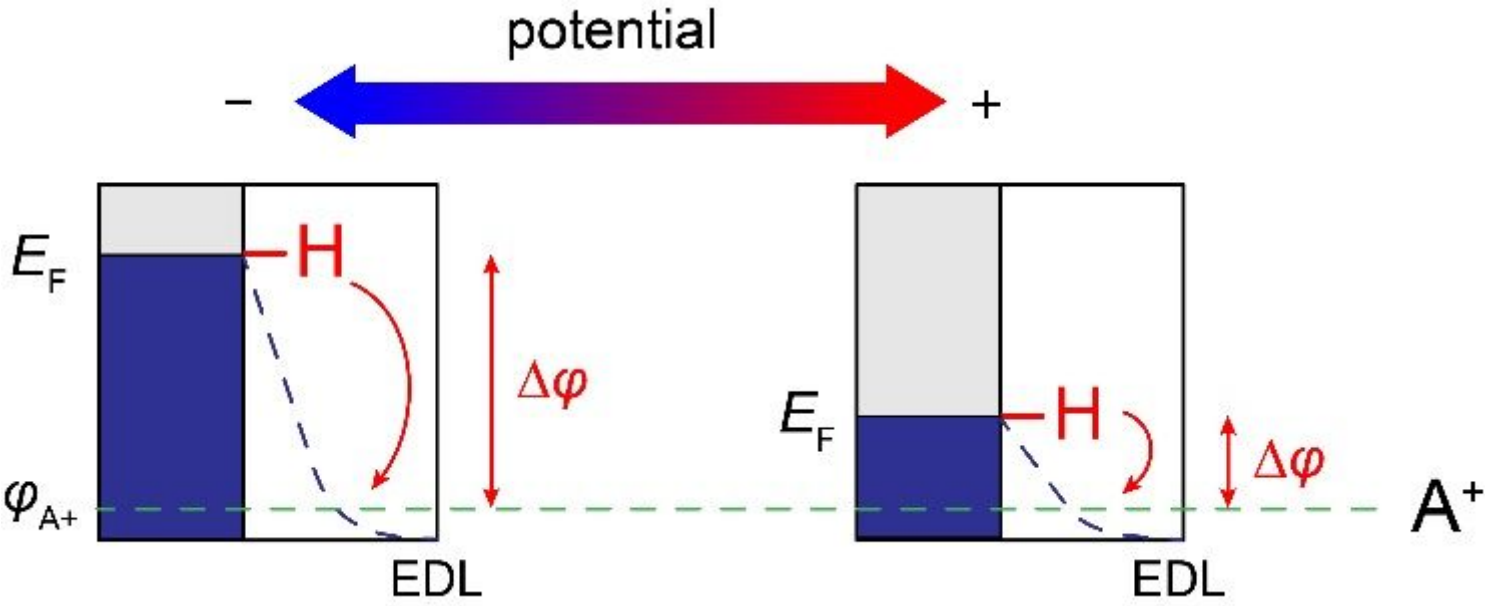

Figure 4

Schematic diagram of interfacial hydride transfer. A qualitative relationship between electrode potential and hydride transfer reactivity of surface M–H, where a more negative potential increases the driving force for hydride transfer by increasing the electrostatic potential drop at the interface. E_F = potential at Fermi level; EDL = electrical double layer; ϕ_{A+} = electrostatic potential of A^+ in solution; $\Delta\phi$ = electrostatic potential drop at the interface.

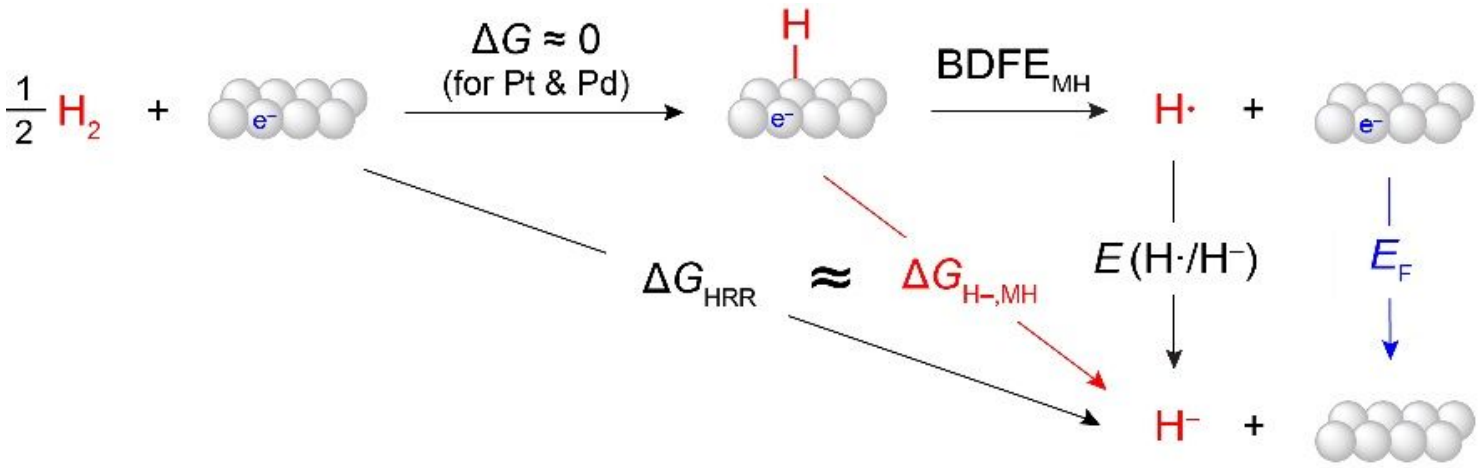

$$\Delta G_{\mathrm{H-,MH}} = \mathrm{BDFE_{MH}} - FE(\mathrm{H\cdot/H^-}) + FE_{\mathrm{F}} \quad (7)$$

Figure 5

Thermochemical cycle of HRR and surface hydricity. Eq. 7 shows the quantitative dependence of thermodynamic hydricity of surface M−H on electrical polarization. Note that eq. 7 can be generally applied to interfacial hydride transfer reactions beyond HRR. ΔG_{HRR} = free energy change of HRR. $\Delta G_{\mathrm{H-,MH}}$ = thermodynamic hydricity of surface M−H. $\mathrm{BDFE_{MH}}$ = bond dissociation free energy of surface M−H. $E(\mathrm{H\cdot/H^-})$ = standard reduction potential between solvated hydrogen atom and solvated hydride ion.

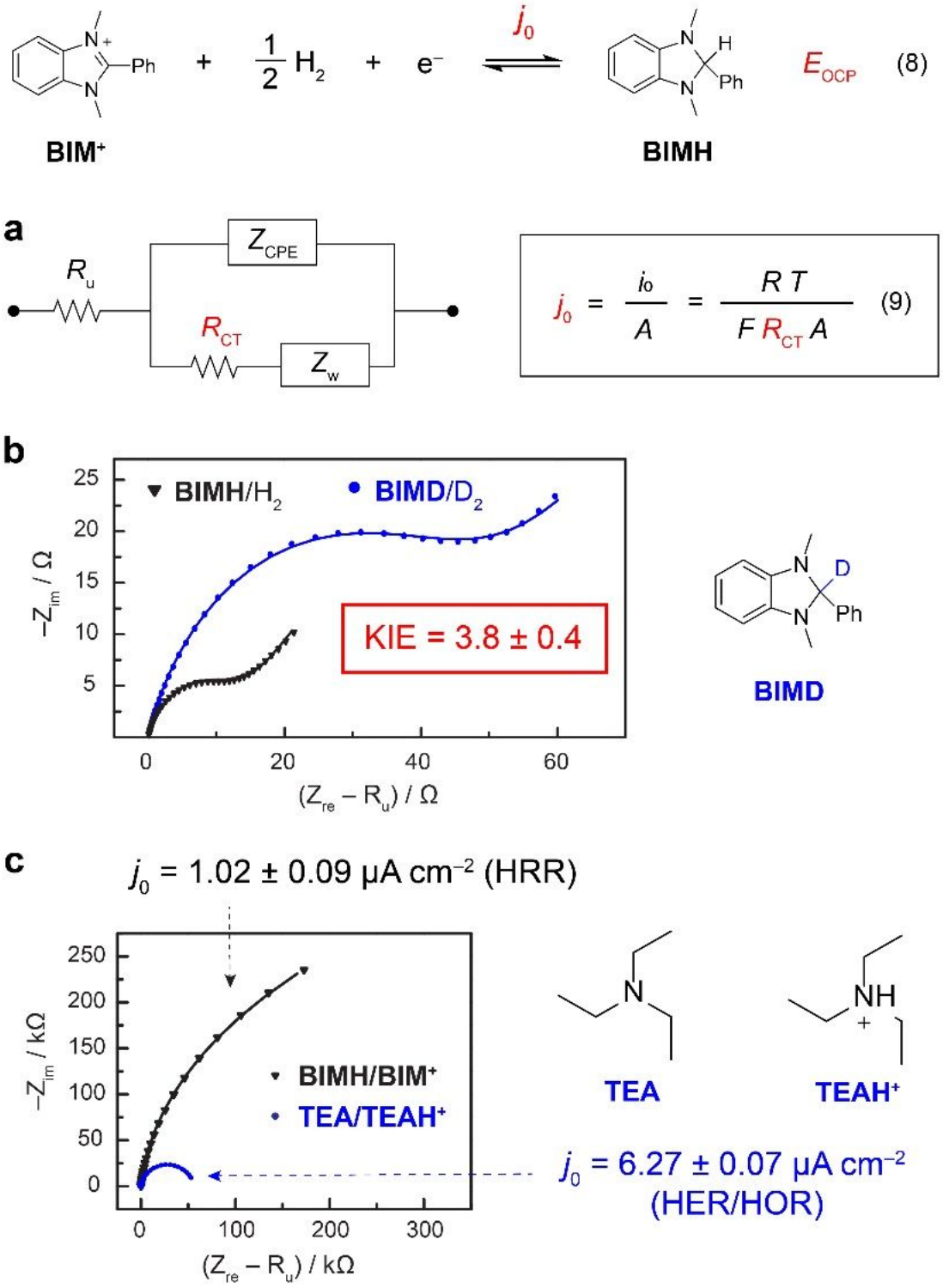

Figure 6

Kinetics studies. Exchange current density (j_0) of HRR of **BIM$^+$/BIMH** was measured at equilibrium potential (E_{OCP}, eq. 8) by electrochemical impedance spectroscopy (EIS). **a**, A Randles circuit containing Warburg impedance (Z_W) was used as the equivalent circuit for modelling the measured Nyquist plots, and j_0 was calculated using eq. 9. R_u = solution resistance; R_{CT} = charge transfer resistance of HRR; Z_{CPE}

= constant phase element for double layer capacitance; i_0 = exchange current; A = electrochemically active surface area (ECSA) of the electrode. **b**, Nyquist plots obtained by EIS measurements and kinetic isotope effect (KIE) of HRR. Black triangles and blue circles are experimental data and solid lines are fitted curves modelled by the equivalent circuit. **c**, Comparison of kinetics between HRR of **BIM^+/BIMH** and HER/HOR of **$TEAH^+$/TEA**. See SI for detailed EIS experimental parameters.

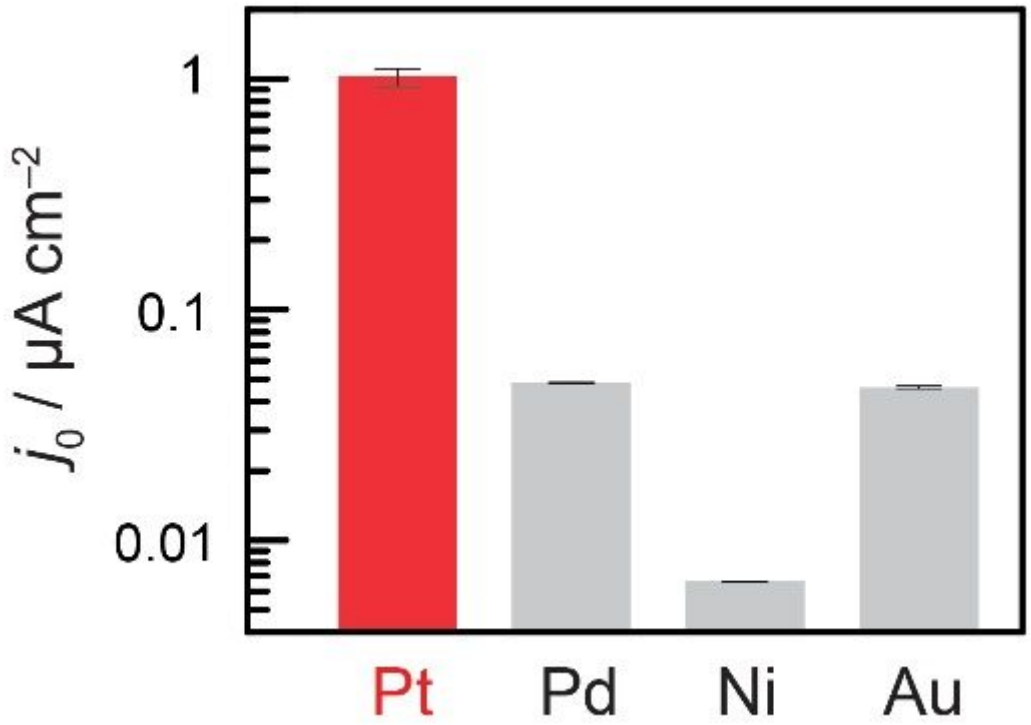

Figure 7

Effect of electrode material on HRR kinetics. Comparison was made by using j_0 values of eq. 8 in Fig. 6, which were measured by EIS experiments on Pt, Pd, Ni, and Au planar electrodes. See SI for experimental details.

Supplementary Files

This is a list of supplementary files associated with this preprint. Click to download.

- SIhydride20221012.pdf